A Biomechanical Model of Traumatic Contusional Injury Produced by Controlled Cerebrocortical Indentation in Sheep

Jeffrey K. Dutschke, Robert W. G. Anderson, Baptiste Sandoz, John W. Finnie, Jim Manavis, Tetsuya Nishimoto, Tom C. Morris, Adam J. Wells, Renée Turner, Robert Vink

Abstract A biomechanical model of traumatic contusional injury was used to map axonal damage and neuronal reaction proximal and distal from the contusion. The model uses a precisely controlled and characterised dynamic indentation of the cerebral cortex of anaesthetised sheep. The indentation (16.15-16.50 mm deep; contact speed 1.2 - 1.24 m/s) is made through a 20 mm craniotomy in the frontal bone. The brain is then perfused-fixed after 6 hours and sectioned at 5 mm intervals. Immunohistochemistry was used to detect axonal injury and neuronal reaction. Quantitation of injury was by an automatic counting algorithm applied to micrographs of each entire section. These maps were cross-checked with manual counts. The injury was characterised by well-defined zones radiating from the impact point; these were a region of haemorrhagic and necrotic tissue, subadjacent penumbra of axonal injury, and distal multi-focal and diffuse areas of neuronal positivity. The model includes precise characterisation of the contact load and the pattern of injury. This will allow future finite element modelling to be used to explore quantitative relationships between several forms of neural damage and the dynamics of the tissue deformation in a finite element model of the insult.

Keywords **Brain Injury, Controlled Cortical Indentation, Axonal Injury, Sheep**

I. INTRODUCTION

Controlled Cortical Indentation (CCI) [1] is a technique that can be used to produce repeatable brain injury. CCI has been used extensively to study the response of the brain to mechanical trauma, most often in the rodent brain [2-4] but also in the pig brain [5,6] and the monkey brain [7]. CCI can produce several types of brain injury including cerebral contusion, axonal injury and haemorrhage [8].

Although the mechanics of the CCI model may have less in common with injurious human head impacts than models that attempt to replicate inertial head loads, the CCI model may still provide important insights into the relationship between the mechanics of brain tissue deformation and resulting injury [3]. Importantly, unlike our previous finite element studies of sheep brain injury [9], the CCI technique leaves the head stationary, and the indentation can be controlled in respect of the location and direction, speed and depth of penetration. These advantages of a CCI model simplify the process of setting boundary conditions for further numerical modelling. Hence, CCI models are amenable to precise control and characterisation due to the simplicity of the loading mechanism. Cortical indentation produces regions of deformation in the brain and these may be related to those deformations that might occur in response to external loads, including rotational loads that can occur in human head impact. The study of the relationships between tissue deformation in the CCI model and resulting injury can therefore be used as one element of ongoing efforts to validate finite element models of brain injury, and define mechanical injury thresholds at the tissue level.

As a biological analogue, the sheep brain has the advantage of being a large and gyrencephalic brain, like that of the human brain, although the arrangement of the neuraxis is different. We have previously used the sheep as a model for human head injury [9-11]. In those studies, the anaesthetised sheep was subjected to a lateral head impact from a humane stunner. Anderson instrumented the impactor and the head of the sheep in order to measure and characterise the mechanics of the impact and the head of the animal. He went on to make a finite element model of these impacts to characterise the tissue mechanics that lead to injury [9]. One limitation of the model was that, despite the biomechanical characterisation of the impact, the dynamic

[1]Jeffrey K. Dutschke, Centre for Automotive Safety Research, University of Adelaide (1) Robert W. G. Anderson (1), Baptiste Sandoz (1), John W. Finnie , University of Adelaide (2), Jim Manavis (2), Tetsuya Nishimoto Nihon University, College of Engineering (3) , Tom C. Morris (1), Adam J. Wells (1), Renée Turner (1), Robert Vink, Sansom Institute for Health Research, University of South Australia(4)

response of the sheep head to the impact was difficult to control and hence to reliably repeat.

The aim of the present study was to develop a precise cortical indentation model brain injury using the living anaesthetised sheep to induce injuries that are analogous to those seen in human traumatic brain injury. The precision in the model is a consequence of the control and measurement of the indentation and the characterisation of the spatial distribution and density of the resulting pathology. These aspects of the model were to be sufficient to allow detailed reproduction of the CCI model using computational finite element methods, with a longer term aim that the computational model would elucidate the relationships between the mechanics of the tissue deformation and the resulting pathology.

In the present paper, the objective was to characterise the mechanics of the CCI impact to the sheep brain, characterise its repeatability, and to produce detailed maps of injury density across the brain volume.

II. METHODS

The following protocol was approved by both animal ethics committees of the University of Adelaide and SA Pathology. Two-year-old Merino wethers were used (N = 4). The animals were anaesthetised for the duration of the experimental procedure until termination without, at any time, regaining consciousness. Anaesthesia was induced with 4% isoflurane (via face mask) in 5L/min oxygen and 20ml Thiopentone (IV), and maintained with 2% isoflurane (via ET tube) in 5L/min oxygen and 2ml/hr ketamine (IV).

The indentation device was custom-built for the study. It consisted of an aluminium rod that had a diameter of 15 mm and a spherical end with a radius of 9 mm. The motion of the rod was controlled by a programmable electromagnetic motor (Linmot , Switzerland). The control system allowed the speed of the indenter on impact, and the depth of indentation to be precisely controlled. A diagram of the impact setup is shown in Figure 1. To minimise any relative motion, both prior to and during the impact, the sheep and the motor were attached to an aluminium frame that was clamped to the surgical table.

A 20 mm craniotomy was performed on the frontal bone above the frontal cerebral cortex of the right hemisphere to expose the brain. The dura was cut and retracted for the indentation. The site was selected based on a desire for consistency between experiments, and for easy surgical access. The position of the craniotomy was measured within an anatomical coordinate system. The coordinate system was defined by three anatomical points: the notches of the zygomatic processes of the malar bones and the point of lambda junction (which is the confluence of the sutures of the parietal and frontal bones). The general position of the craniotomy and the location of the anatomical points for the coordinate system are shown in Figure 2.

The indentation device was positioned above the craniotomy and the positions of the head and the device were adjusted so that the axis of the indentation motion was perpendicular to the surface of the brain. The tip of the indenter was positioned so that it was within 1 mm of the surface of the brain. This distance was the smallest unit of pre-position adjustment possible from the motor. This position provided a zero datum for the indentation control system.

The relative positions of the skull and the craniotomy, along with the axis of motion of the indentation rod, were measured prior to impact with a 3D coordinate measurement machine (Microscribe 3DX, Immersion Corporation) that had an accuracy of 0.38 mm. These measurements were taken immediately prior to lowering the indentation rod to the surface of the brain.

The indentation control system was programmed to raise the indentation rod 250 mm from its zero datum after which the rod was accelerated, under control of the motor toward the surface of the brain. The controller decelerated the rod so that the target speed of the rod, on contact with the brain surface, was 1.2 m/s, reducing to zero in 15 mm of travel (the indentation). The indentation rod continued to be accelerated away from the surface of the brain after peak indentation so that it quickly withdrew, returning to a position

approximately 250 mm away from the brain surface. Contact between the indentation rod and brain surface lasted approximately 60 ms.

High speed video was also used to record each experiment.

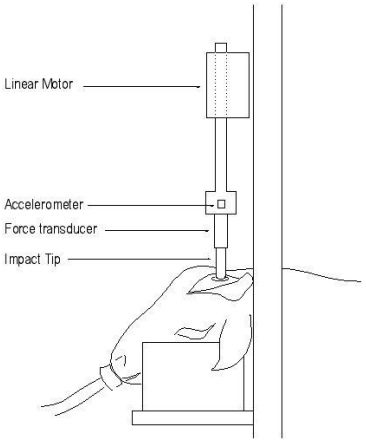

Fig 1. Experimental setup showing the ventilated animal, impact device and measurement equipment.

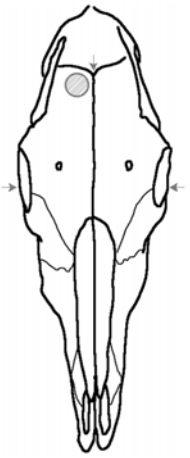

Fig 2. The 20 mm diameter crainiotomy, marked with a grey cross-hatched circle. The location of the crainiotomy was measured with reference to an anatomical coordinate system based on the anatomical points marked with arrows.

A. Position and velocity measurement

The speed and position of the indenter tip was measured directly during the procedure. Thirty-two data points were collected from the Linmot at a sampling frequency of 500 Hz over the duration of the contact between the tip of the indentation rod and brain. The number of data points was limited by the capacity of the Linmot system. The system was programmed to collect data points that included the period ranging just prior to first contact until just after final contact.

B. Accelerometer and force transducer measurement

The dynamics of the indenter (acceleration and contact force) were measured using an accelerometer fixed to the rod and a force transducer was placed between the tip of the indentation rod and the motor. Data from the accelerometer and the force transducer was sampled at 20000 Hz and filtered with an 8th order Butterworth filter at 100 Hz.

The force at the tip of the indenter was calculated by subtracting from the transducer measurement the inertial force created by the acceleration of the mass of the indenter rod forward of the transducer.

This technique for estimating the force on the tip was validated by running the indentation device against a mounted calibrated load cell. The force recorded on the struck load cell was within 2 N of the force estimated by the load cell attached to the striker.

C. Post-indentation procedures

After indentation, the dura and craniotomy were surgically repaired. The animals remained in the sphinx position anaesthetised and ventilated for exactly 6 hours. Blood gases were regularly monitored to ensure that no hypoxic or hypercarbic episodes occurred. After 6 hours, the animals were killed by perfusion fixation of the brain.

D. Pathology

The skull and brain were removed for further analysis. The brain remained in situ in the cranial cavity for 24 hours to ensure complete fixation. It was then was removed and immersed in 10% buffered formalin for 7 days. Coronal sections of brain were cut at 5mm intervals and embedded in paraffin. They were then cut into 6 µm sections for routine histological examination and duplicate sections were cut for immunohistochemistry.

Beta amyloid precursor protein (APP) is a sensitive early marker of axonal injury. APP is normally transported by fast axoplasmic transport in histologically undetectable quantities, but it accumulates rapidly in damaged axons proximal to the site of injury. APP may be stained and becomes visible by light microscopy 1.75 to 3 hours post-injury [12]. Neuronal perikaryal APP immunopositivity probably represents a non-specific, acute stress response to trauma [13].

For APP immunohistochemistry, a monoclonal antibody to APP (clone 22C11, gift from Prof C Masters, University of Melbourne) was used in a standard streptavidin-biotinylated immunoperoxidase technique. In brief, APP antibody was applied at a dilution of 1:1000, then a biotinylated anti-mouse secondary reagent (Vector Laboratories, Burlingame, CA, USA, catalogue # BA-200) was applied. Slides were then incubated with a streptavidin-conjugated peroxidase tertiary reagent (Pierce, Pasadena CA, USA, catalogue # 21127). Labelling was visualized using 3,3 diaminobenzidine tetrahydrochloride (DAB). Finally, sections were counterstained with haematoxylin.

Analysis of the Hematoxylin and eosin (H&E) stained sections was done via light microscopy by one of the authors (Finnie). Analysis of the APP stained sections was performed electronically after scanning at 40× magnification (NanoZoomer, Hamamatsu). Because of the size of the brain sections and the physical limitations of the scanning machine, it was not possible to fit complete brain sections on single slides to permit scanning, and each section was split along the midline of the horizontal plane.

Automatic counts of injury were obtained using the method devised by one of the authors (Dutschke) and described in [14]. Briefly, this involved applying a color deconvolution method [15] to separate the color of DAB stain from the background stain on non-overlapping image tiles obtained at 10 times magnification. A pixel intensity value of 200 (unsigned 8-bit integer) was used as the threshold of DAB positivity from an inverted deconvoluted image. Contiguous clusters (greater than 5) of the positive pixels were then aggregated over a 800×800 pixel (0.53 mm^2) square grid to provide an estimate of injury density.

Images from each brain section were overlaid with contours of cluster density to show a map of high and low injury density.

These maps, along with the original scan data, were then reviewed by pathologists to grade the injury observed within the tissue sections. A subjective scale of 1+ to 3+ was used to quantify axonal and neuronal injury. The entire coronal section of the brain was scanned and where there were APP immunopositive neurons or axons, these were graded as 1+ to 3+, where 1+ indicated areas of relatively few immunopositive elements and 3+ indicated areas of numerous APP immunopositive axons or neurons.

III. RESULTS

All craniotomies were performed on the right frontal bone at the positions shown in Table 1. There are small differences in craniotomy locations and indenter angle and these are shown in the table.

Table 1.
Location of centre of crainiotomy relative to a coordinate system defined by three anatomical points: the notches of the zygomatic processes of the malar bones and the point of lambda junction. The origin of the coordinate system is at the lambda junction, the x axis parallel to the zygomatic notches, and all three of these points lie on the y=0 plane. Distances measured in mm and angles in degrees.

Sheep	To Right (parallel to line between eye notches)	Distance from notch to centre of craniotomy	Coordinates of craniotomy center (x,y,z)	Direction from notch	Angle between indenter and sagittal plane of head
A	12.9	15.8	-12.9, 1.2, 9.0	rostral	36
B	11.5	12.8	-11.5, 3.5, 4.7	rostral	22
C	13. 0	13.7	-13.0,-1.3,4.1	caudal	31
D	10.9	16.4	-10.9,8.9,8.4	rostral	32

A. Impact kinematics

Figure 3 shows the impact sequence from when the striker first contacts the brain, then reaches maximum depth before lifting away from the brain again. The kinematics of each impact, as measured by the accelerometer and/or the motor assembly, are shown in Figure 4.

The speed of the indenter at the time of first contact ranged between 1.20 and 1.24 m/s. The depth of impact was between 16.15 and 16.50 mm. The data for these parameters for each of the impacts is shown in Table 2. All data lie within 5% of the maximum value of each parameter.

B. Reaction Force on the indenter

The reaction force between the brain and the tip of the indenter for each sheep is shown in Figure 5. The peak reaction force ranged between 22 and 24 N as shown in Table 2. The peak force occurred while the indenter was approximately two-thirds of its maximum distance into the brain. The reaction force dropped to near zero at maximum displacement. Except for a slight tensile force as the indenter began to be withdrawn, the force remained near zero while the indenter was being withdrawn from the brain. This behaviour is consistent with impact behaviour with a material of low stiffness and high damping.

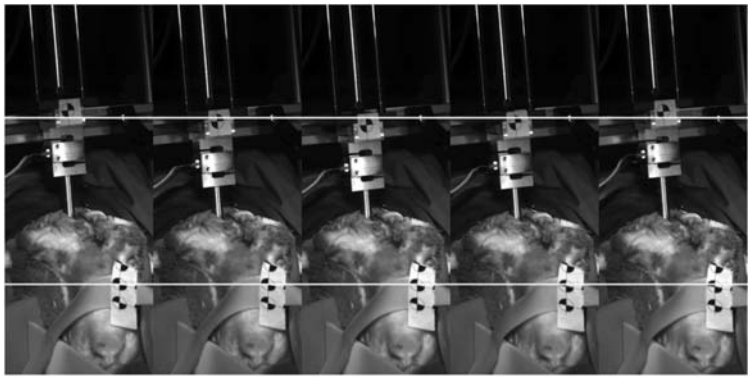

Fig 3. Impact sequence of Sheep B. Frames separated by 15 ms. The two horizontal lines indicate stationary positions of the indentation rod (upper line) and the sheep head (lower line). The motion of the indentation rod is indicated by the movement of the upper target. The sheep's head remains stationary during the impact as indicated by the stationary position of the lower targets.

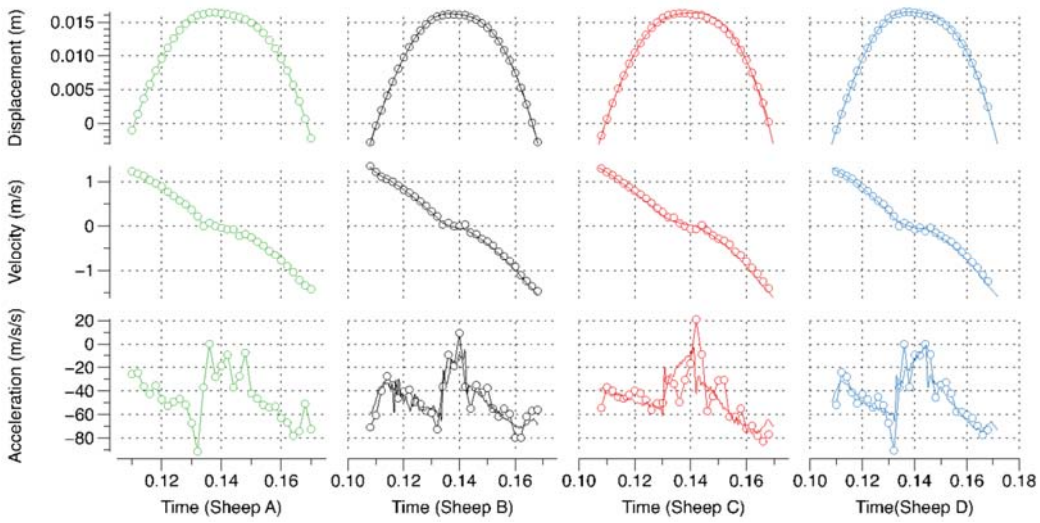

Fig 4. Kinematic data derived from the accelerometer (solid line) and from the electromechanical motor (line with markers). The accelerometer data was integrated to obtain the velocity and displacement; the acceleration data for the electromechanical motor is determined by differentiation of its velocity data. A displacement value greater than 0 indicates contact between the brain and indenter.

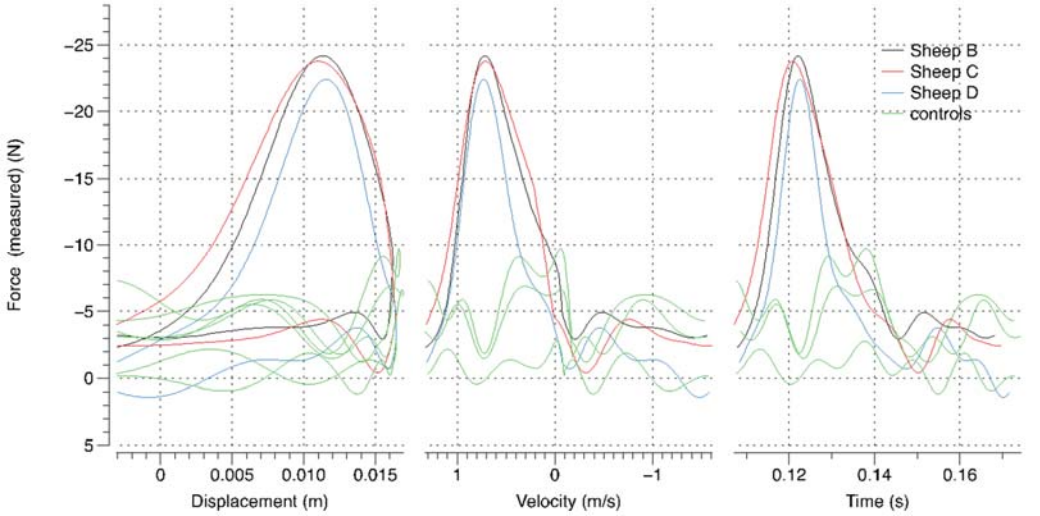

Fig 5. Reaction force between the tip of the indenter and the brain (negative indicates compressive force). The reaction force measured during trial impacts (with no impact) are also shown. No force measurement was obtained in Sheep A.

Table 2
Peak values measured during each experiment

Sheep	Impact Velocity (m/s)	Impact Depth (mm)	Peak force (N)
A	1.24	16.41	Not measured
B	1.20	16.15	24.2
C	1.23	16.32	23.8
D	1.20	16.50	22.4

C. Injury Response

Routine haematoxylin and eosin (H&E)-stained sections, 6h post-impact, indicated that the indenter produced a severe, well-defined, haemorrhagic and necrotising wound track (contusion/laceration) through the cerebral cortex, which sometimes extended into the digitate white matter. Within this penetrating wound track, there was multifocal to coalescing haemorrhage with widespread necrosis and disruption of the cortical parenchyma, attended by some detached and in-driven cortical fragments. The injured cortex also showed extensive extravasation of plasma proteins, spongy change of the neuropil, and many pyknotic or karyorrhectic glial nuclei, although some viable astrocytes with swollen nuclei were found. There was also neutrophilic infiltration. In the wound track, there was marked neuronal loss, but some ghost neuronal profiles or neurons showing shrunken, hypereosinophilic cytoplasm (red neurons) and often nuclear hyperchromasia or pyknosis were found. In the cortical wound track penumbra, there were many red neurons, characterised by hypereosinophilic cytoplasm and sometimes nuclear hyperchromasia, with enlarged, non-staining, perineuronal spaces. Many of these red neurons were markedly elongated (plastic creep) and oriented in a similar plane, reflecting the line of force of the applied traumatic insult, while some had more triangular or rounded cell outlines and shrunken cytoplasm. Intervening neurons either appeared normal or were elongated with basophilic cytoplasm and nuclear hyperchromasia. In these cortical areas, many astrocytic nuclei were swollen, there was mild neutrophilic infiltration, and sometimes perivascular lakes of extravasated proteinaceous material. Subarachnoid haemorrhage often extended some distance from the wound track.

The cytoplasm of the majority of red neurons in the wound track penumbra, and that of the few remaining viable neurons within the wound track, was almost invariably uniformly APP-immunopositive, suggesting that these neurons were still viable and able to react to traumatic stress. A few APP-positive axons were found in less severely damaged areas of the wound track, but they were abundant, and randomly distributed, in the track penumbra and, more particularly, in the white matter tracts subjacent to the wound track. Neurons of the central grey matter in the same coronal plane as the wound track, and in ipsi- and contralateral cortices, were also frequently APP-immunopositive, but APP-positive axons diminished in number with increasing distance from the wound track, suggesting that the threshold for APP-immunoreactivity was much less in neurons than axons. Control tissue subjected to the same immuno histological processes show only a very small number of weakly APP-immunopositive neuronal cell bodies and no axonal injury [10,11]. Some of the features of the pathology are shown in Figure 6.

D. Maps of APP positivity (axonal injury)

Maps of the cluster density of DAB stained, APP positive tissue in the coronal sections nearest the site of impact are shown in Figure 7. Contour levels are at 25, 50, 100, 200 and 500 counts per grid division. Contours of high axonal injury follow tracks of white matter, while neuronal injury is found in areas of grey matter. False positive contours are found in (especially) the choroid plexus, and in other areas including places where tissue has folded over itself on the slide, or where there is a mark on the glass slide. Injury maps for other coronal sections (each separated by 5 mm) are provided in the Appendix.

IV. DISCUSSION

The apparatus used for the experiments was shown to be highly controllable giving a repeatable impact pulse. In the four experiments conducted here, the speed of the impactor and depth of impact in each experiment were closely matched. Precise control of the electromechanical linear motor is achieved with constraints placed on both the position and velocity. Unlike some other controlled cortical impact apparatus [4] the position and the velocity in the present study were controlled throughout the impact. Consequently, the impactor is brought to a soft stop at the bottom of the stroke using controlled deceleration that is powered by the motor. Other techniques come to a hard stop at the limits of travel of the apparatus. While we have only reported a simple impact scenario, the apparatus makes it possible to program a complex impact that has, for example, multiple strikes at different depths and speeds over a specified time interval.

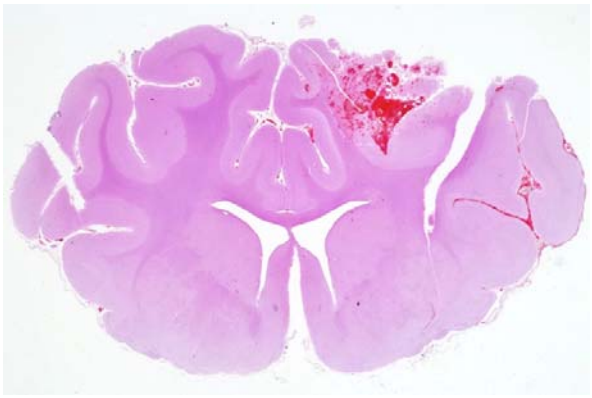

Fig 6(a). Cortical impact contusion, with midline shift of the brain, and subarachnoid haemorrhage at right of image.

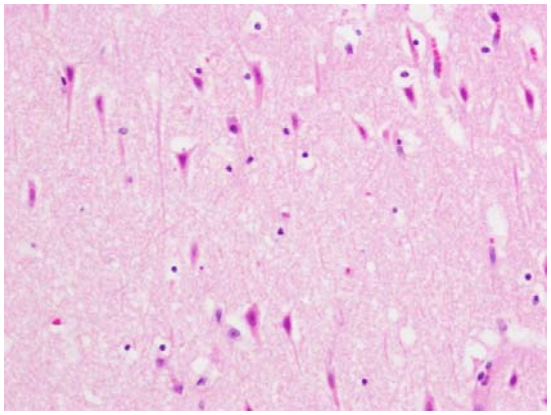

Fig 6(b). Many cerebrocortical neurons in the wound track penumbra are markedly elongated (`plastic creep') with hypereosinophilic cytoplasm (`red neurons').

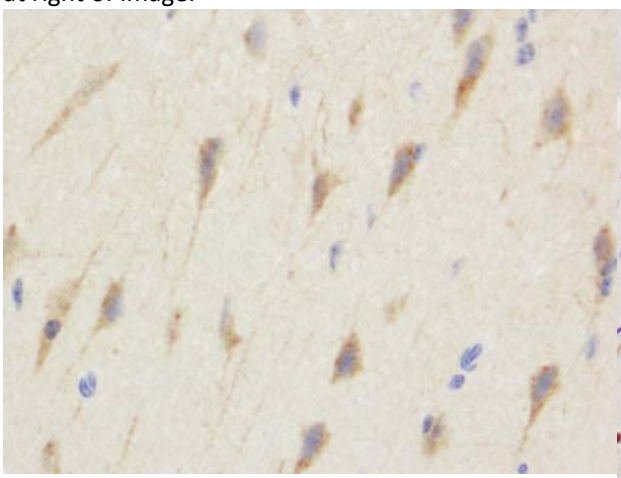

Fig 6(c). The neurons shown in Figure 6(b) exhibit APP-immunopositivity

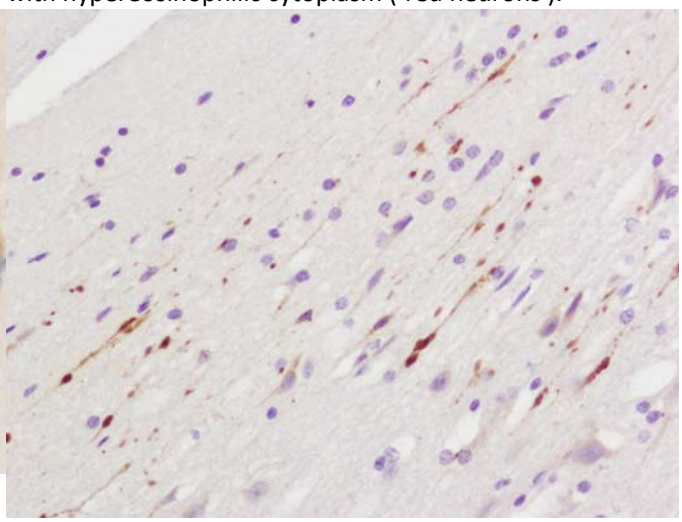

Fig 6(d). APP-immunoreactive damaged axons in the contusion penumbra

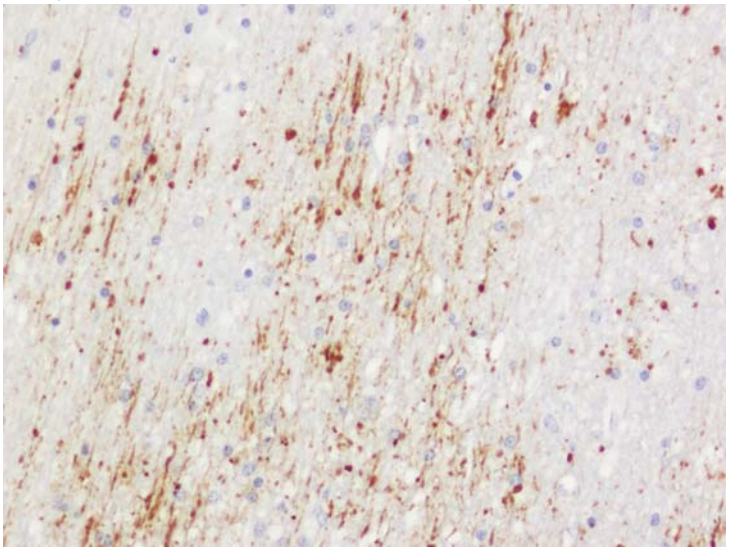

Fig 6(e). Abundant APP-immunopositive damaged axons, mostly running longitudinally in the same direction, in a large white matter tract subjacent to the wound track; uninjured axons are not labelled by this immunohistochemical technique.

Fig 6. Pathology found in the sheep brains

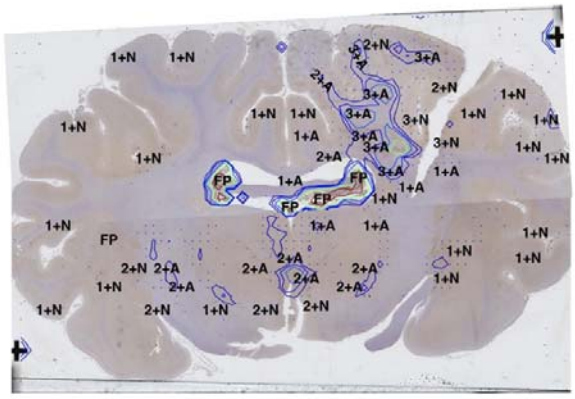

Fig 7(a). Sheep A, coronal level 5

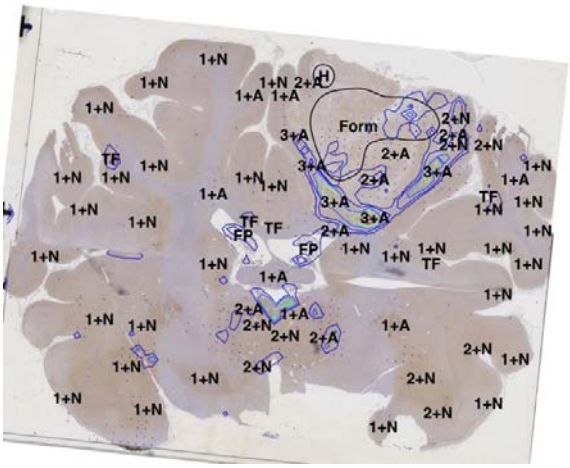

Fig 7(b). Sheep B, coronal level 5

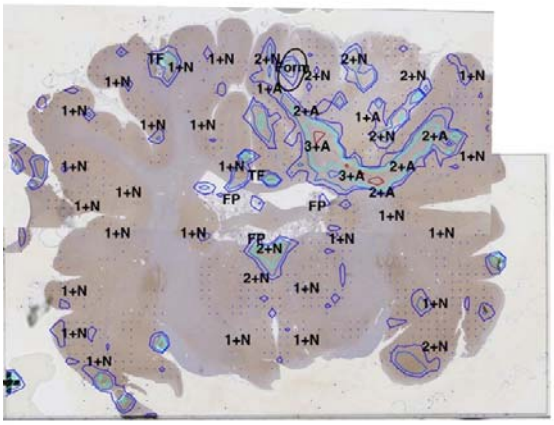

Fig 7(c). Sheep C, coronal level 5

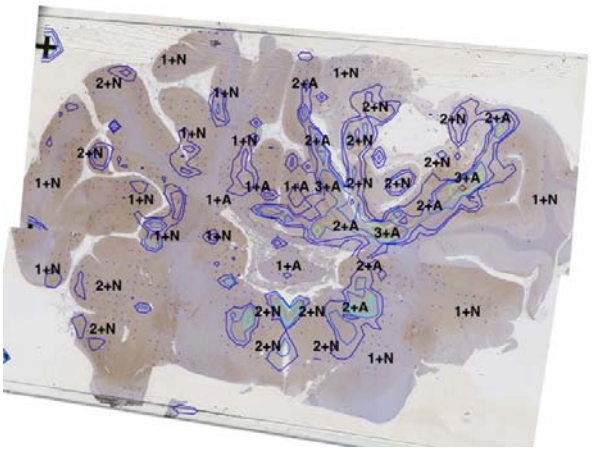

Fig 7(d). Sheep D, coronal level 5

Fig 7. Representative injury levels from each sheep. Contour levels are at 25, 50, 100, 200 and 500 counts per grid division. Dots show grid points with between 5 and 25 counts. Manual pathology markings are as follows: x+A indicates axonal injury at level x, x+N indicates neuronal injury at level x. Form represents an area of formalin pigmentation, H indicates a hole, FP indicates a false positive (due to extraneous DAB build up on the slide) and TF indicates an area of tissue folds. All sections for each sheep are shown in the appendix.

There were 3 principal features of the brain injury produced by the indenter:

1. a contusion at the impact site, which was comprised of parenchymal necrosis and haemorrhage, abetted by tissue disruption (laceration);
2. a contusion penumbra of less severe neuronal, glial and axonal injury; and
3. neuronal reaction and axonal injury distant to the impact site, with the former showing greater and more widely distributed APP immunopositivity, suggesting that the threshold for neuronal reaction detected by APP immunohistochemistry may be lower than that for axonal injury.

The injuries suggest distinct radial zones of injury that may correspond to the regions of differentiated levels of tissue stress. The microscopic features of cellular distortion suggest differentiated areas of tissue strain. We hypothesise that these differentiated areas of tissue stress/strain will be quantifiable by finite element modelling.

There were, however, easily observable, but difficult to quantify, differences in injury distributions between the animals. Qualitatively, the extent and magnitude of the injury was different in each animal. Additionally,

while the presence of a penumbra of axonal injury was consistent in each animal, its extent was variable. This variability may have been due to the differences in impactor position, or it may have been a result of each individual subject response to the impact or the variability in the anatomy of each sheep. We expect that it is questions like these that may be examined by future finite element modelling of these experiments.

The injury patterns that were found in this study, however, are consistent with the patterns of injury described in porcine models of CCI [5,6]. These porcine models also showed a local area of necrosis and haemorrhage surrounded by a penumbra of axonal and neuronal injury.

While the pathology of the injury observed in this study has been described subjectively in this study, the injury expression was also automatically and quantitatively rated. Locations of injury were identified from scanned sections of the brain tissue with a color deconvolution algorithm [14] adapted from Ruifrok and Johnston [15]. To the authors knowledge, this is the first time this method has been adapted to identify locations of injury and report their densities across a whole brain volume; quantitation of this type has not a common feature of other biomechanical models reported in the literature.

This quantitation method delivers an automatic and high-density approach to describing injury across large sections of brain. However, as highlighted in [14] it is liable to identify false positive locations due to the non-specific staining of the tissue with the DAB. This issue has been mitigated, in this case, with a review of the scans by experienced pathologists to identify true-positive areas of injury and also identify areas that are not injured.

This method of automatic counting combined with qualitative annotation improves upon previously presented maps of axonal injury. The previous methods have relied on coarsely-spaced counts of axonal injury or line diagrams which have also relied on review by pathologists for accuracy. As an example, Anderson et al. [9] used the sector axonal injury score whereby axonal injury was identified in a 4 mm spaced square grid with injury graded into counts of no injury, 1-2 axons, 3 or more axons, and macroscopically visible injury. A similar level of detail has been provided in the annotations provided in this study. Consequently, the method presented here has been subjected to the same level of manual oversight while providing a much greater resolution through the use of the automatic algorithm.

Animal models of injury that include precise biomechanics data collected during experimentation, are ideal for simulation and study using finite element methods. In this study we have described a model for large animal brain injury using direct impact to the brain of a sheep. The highly controlled and measured nature of the impact should prove useful for studying tissue level brain injury criteria as the measurements are designed to be suitable for use in finite element simulations of the impacts.

V. CONCLUSIONS

The controlled and precise cortical indentation of the brains of sheep produced distinct zones of injury radiating from a central contusional wound. These injuries included axonal injury and neuronal reactivity. The dynamics of the insult were characterised and shown to be repeatable and highly controllable. Automatic injury identification through colour deconvolution and clumping was successfully applied across the whole brain volume producing high resolution three dimensional maps of the severity and distribution of axonal injury. The combination of the precisely defined nature of the insult and the maps of injury will be suitable for identifying injury thresholds using the finite element method.

VI. ACKNOWLEDGEMENT

This publication was supported by a grant from the Brain Foundation (http://brainfoundation.org.au).

The Centre for Automotive Safety Research, University of Adelaide, is supported by both the South Australian Department of Planning, Transport and Infrastructure and the South Australian Motor Accident

Commission. The views expressed in this paper are those of the authors, and do not necessarily represent those of CASRs other funding organizations.

VII. REFERENCES

[1] Dixon, C.E., Clifton, G.L., Lighthall, J.W., Yaghmai, A.A., and Hayes, R.L. A controlled cortical impact model of traumatic brain injury in the rat. *Journal of neuroscience methods*, 1991. 39(3): p. 253-262

[2] Brody, D.L., Mac Donald, C., et al. Electromagnetic controlled cortical impact device for precise, graded experimental traumatic brain injury. *Journal of neurotrauma*, 2007. 24(4): p. 657-673

[3] Chen, Y., Mao, H., Yang, K.H., Abel, T., and Meaney, D.F. A modified controlled cortical impact technique to model mild traumatic brain injury mechanics in mice. *Front Neurol*, 2014. 5: p. 100

[4] Lighthall, J.W. Controlled cortical impact: a new experimental brain injury model. *Journal of neurotrauma*, 1988. 5(1): p. 1-15

[5] Alessandri, B., Heimann, A., Filippi, R., Kopacz, L., and Kempski, O. Moderate controlled cortical contusion in pigs: effects on multi-parametric neuromonitoring and clinical relevance. *Journal of neurotrauma*, 2003. 20(12): p. 1293-1305

[6] Manley, G.T., Rosenthal, G., et al. Controlled cortical impact in swine: pathophysiology and biomechanics. *Journal of neurotrauma*, 2006. 23(2): p. 128-139

[7] King, C., Robinson, T., et al. Brain temperature profiles during epidural cooling with the ChillerPad in a monkey model of traumatic brain injury. *Journal of neurotrauma*, 2010. 27(10): p. 1895-1903

[8] Dixon, C.E. and Kline, A.E., "Animal models of acute neurological injuries", pages 385-391, Springer, 2009

[9] Anderson, R.W.G., Brown, C.J., et al. Mechanisms of axonal injury: an experimental and numerical study of a sheep model of head impact. *Proceedings of Proceedings of the International Research Council on the Biomechanics of Injury conference*.

[10] Lewis, S.B., Finnie, J.W., et al. A head impact model of early axonal injury in the sheep. *Journal of neurotrauma*, 1996. 13(9): p. 505-514

[11] Van den Heuvel, C., Blumbergs, P.C., et al. Upregulation of amyloid precursor protein messenger RNA in response to traumatic brain injury: an ovine head impact model. *Experimental neurology*, 1999. 159(2): p. 441-450

[12] Blumbergs, P., Reilly, P.L., and Vink, R., "Greenfield's Neuropathology Eighth Edition 2-Volume Set", CRC Press, 2008

[13] Mattson, M.P. Cellular actions of beta-amyloid precursor protein and its soluble and fibrillogenic derivatives. *Physiological reviews*, 1997. 77(4): p. 1081-1132

[14] Dutschke, J.K., Finnie, J.W., Manavis, J., and Anderson, R. Semiquantitation of Axonal Injury in Traumatically Damaged Brains Using Color Deconvolution. *Applied immunohistochemistry & molecular morphology: AIMM/official publication of the Society for Applied Immunohistochemistry*, 2015

[15] Ruifrok, A.C. and Johnston, D.A. Quantification of histochemical staining by color deconvolution. *Analytical and quantitative cytology and histology/the International Academy of Cytology [and] American Society of Cytology*, 2001. 23(4): p. 291-299

VIII. APPENDIX

Every coronal section for each of the sheep is shown in Figures 8 to 11.

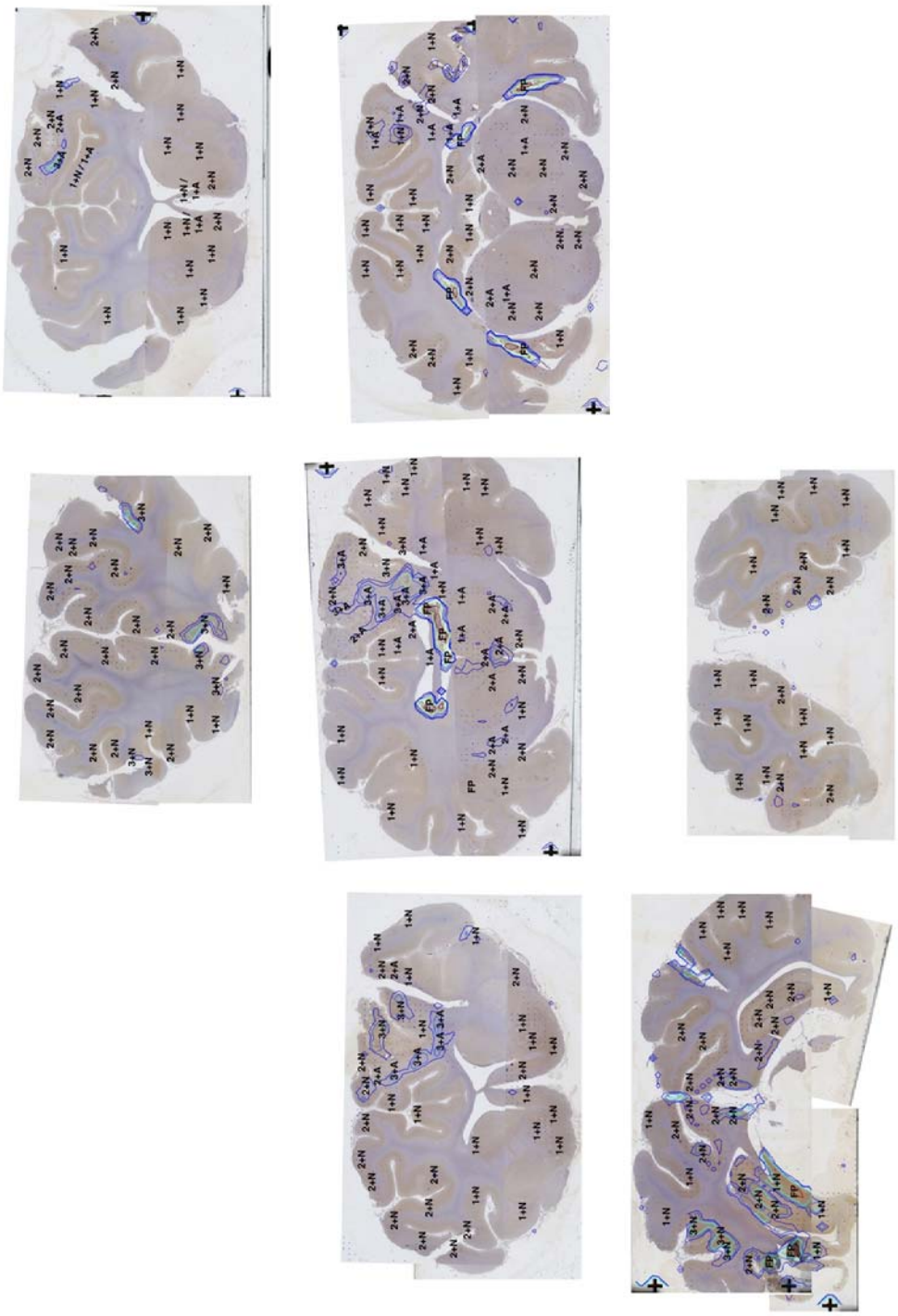

Fig 8. Injury levels on the coronal sections from Sheep A. Left to right, and top to bottom, levels 2 to 8. Each section is separated from each other by 5 mm. Contour levels are at 25, 50, 100, 200 and 500 counts per grid division. Dots show grid points with between 5 and 25 counts. Manual pathology markings are as follows: x+A indicates axonal injury at level x, x+N indicates neuronal injury at level x. Form represents an area of formalin pigmentation, H indicates a hole, FP indicates a false positive (due to extraneous DAB build up on the slide) and TF indicates an area of tissue folds.

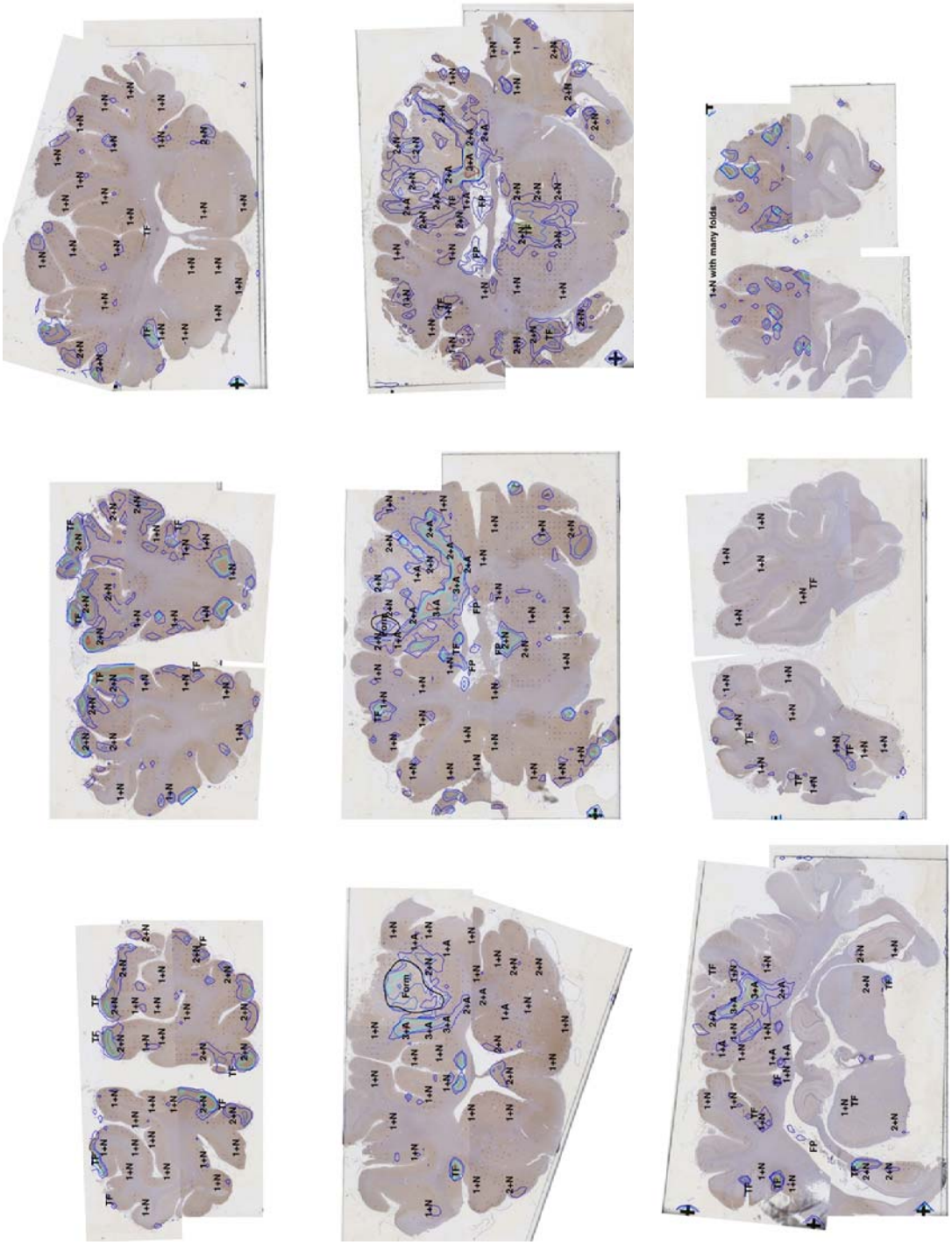

Fig 9. Injury levels on the coronal sections from Sheep B. Left to right, and top to bottom, levels 1 to 9. Each section is separated from each other by 5 mm. Contour levels are at 25, 50, 100, 200 and 500 counts per grid division. Dots show grid points with between 5 and 25 counts. Manual pathology markings are as follows: x+A indicates axonal injury at level x, x+N indicates neuronal injury at level x. Form represents an area of formalin pigmentation, H indicates a hole, FP indicates a false positive (due to extraneous DAB build up on the slide) and TF indicates an area of tissue folds.

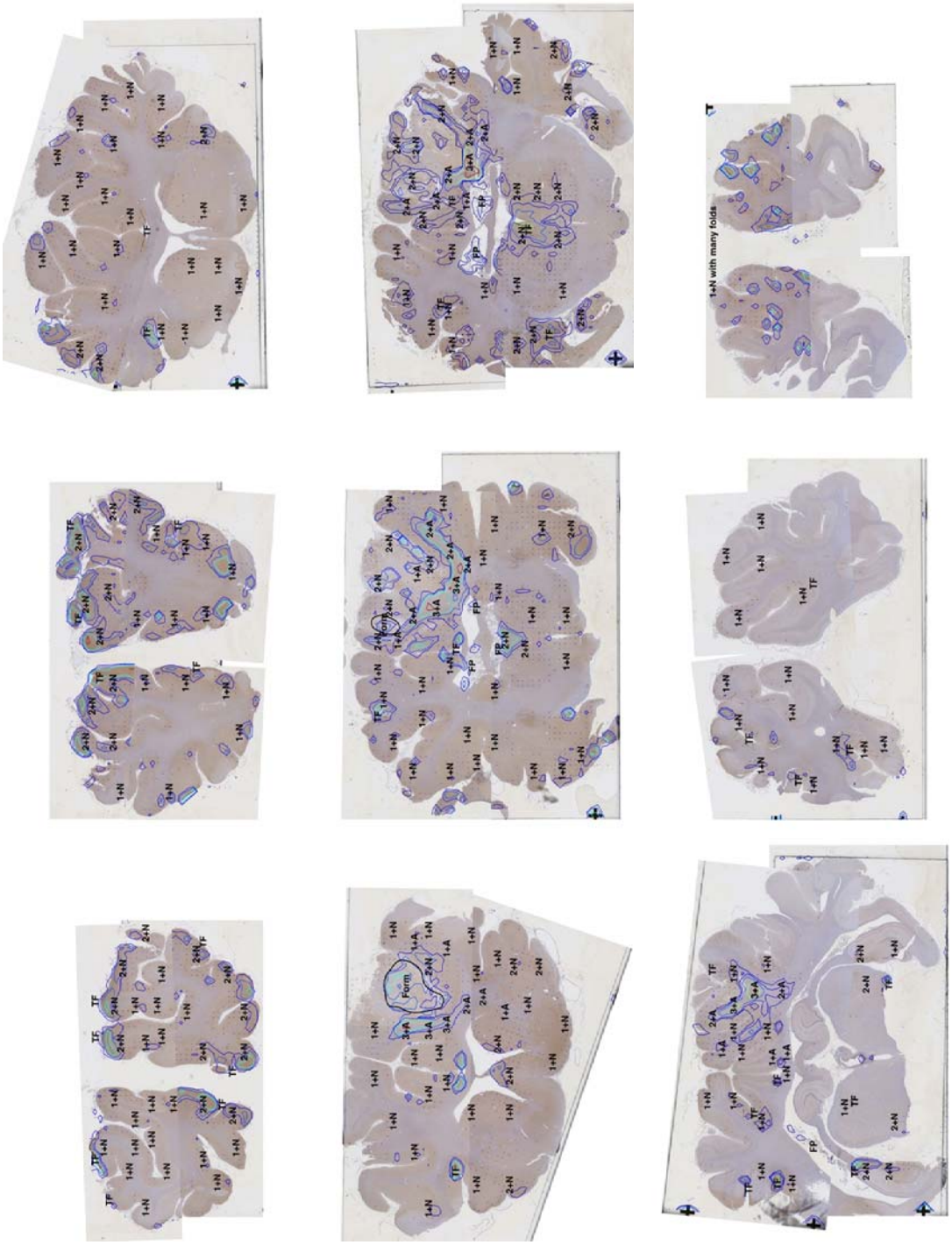

Fig 10. Injury levels on the coronal sections from Sheep C. Left to right, and top to bottom, levels 1 to 9. Each section is separated from each other by 5 mm. Contour levels are at 25, 50, 100, 200 and 500 counts per grid division. Dots show grid points with between 5 and 25 counts. Manual pathology markings are as follows: x+A indicates axonal injury at level x, x+N indicates neuronal injury at level x. Form represents an area of formalin pigmentation, H indicates a hole, FP indicates a false positive (due to extraneous DAB build up on the slide) and TF indicates an area of tissue folds.

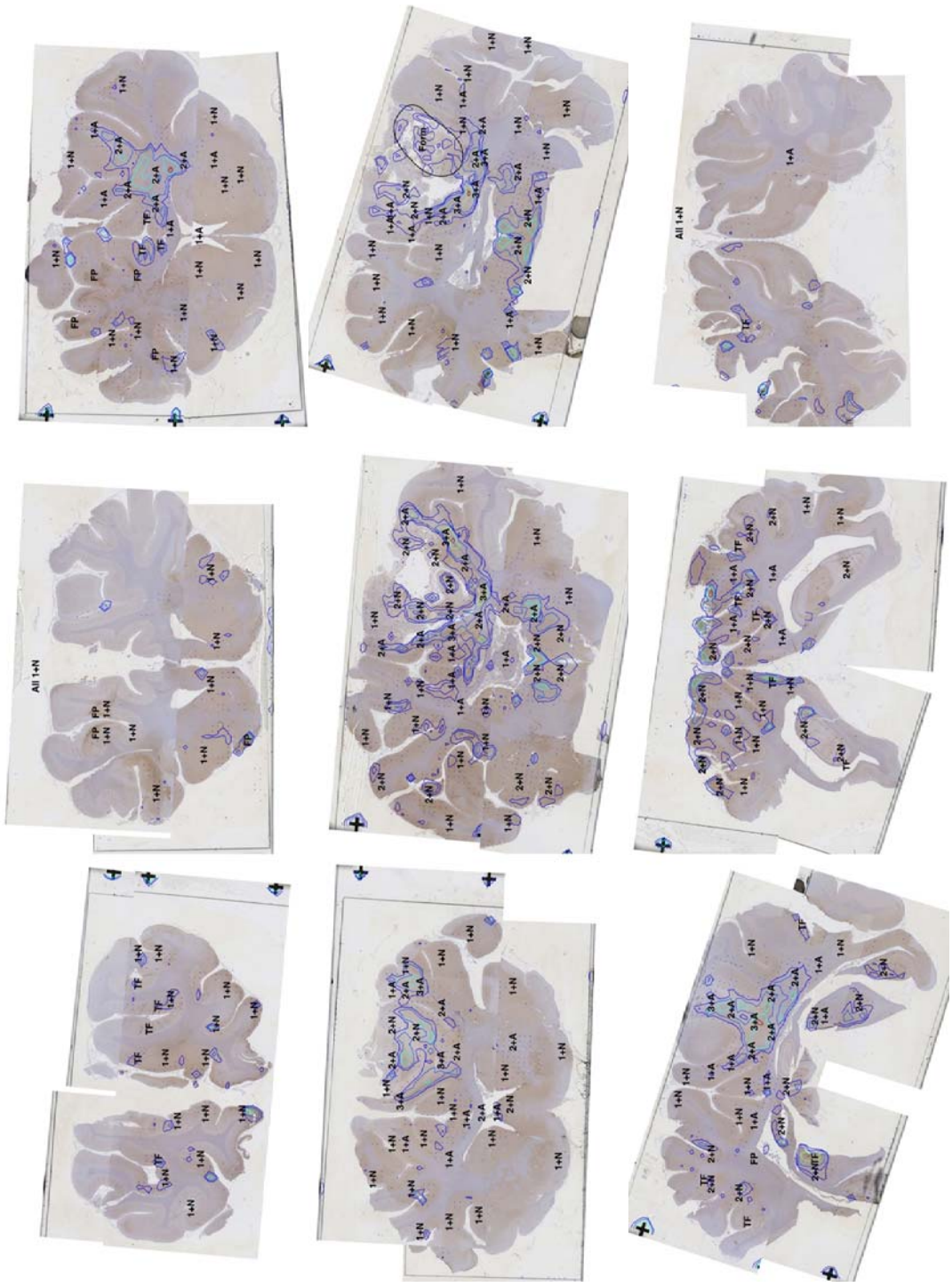

Fig 11. Injury levels on the coronal sections from Sheep D. Left to right, and top to bottom, levels 1 to 9. Each section is separated from each other by 5 mm. Contour levels are at 25, 50, 100, 200 and 500 counts per grid division. Dots show grid points with between 5 and 25 counts. Manual pathology markings are as follows: x+A indicates axonal injury at level x, x+N indicates neuronal injury at level x. Form represents an area of formalin pigmentation, H indicates a hole, FP indicates a false positive (due to extraneous DAB build up on the slide) and TF indicates an area of tissue folds.

Erratum

A Biomechanical Model of Traumatic Contusional Injury Produced by Controlled Cerebrocortical Indentation in Sheep

Jeffrey K. Dutschke, Robert W. G. Anderson, Baptiste Sandoz, John W. Finnie, Jim Manavis, Tetsuya Nishimoto, Tom C. Morris, Adam J. Wells, Renée Turner, Robert Vink

VIII. APPENDIX

Figure 9-

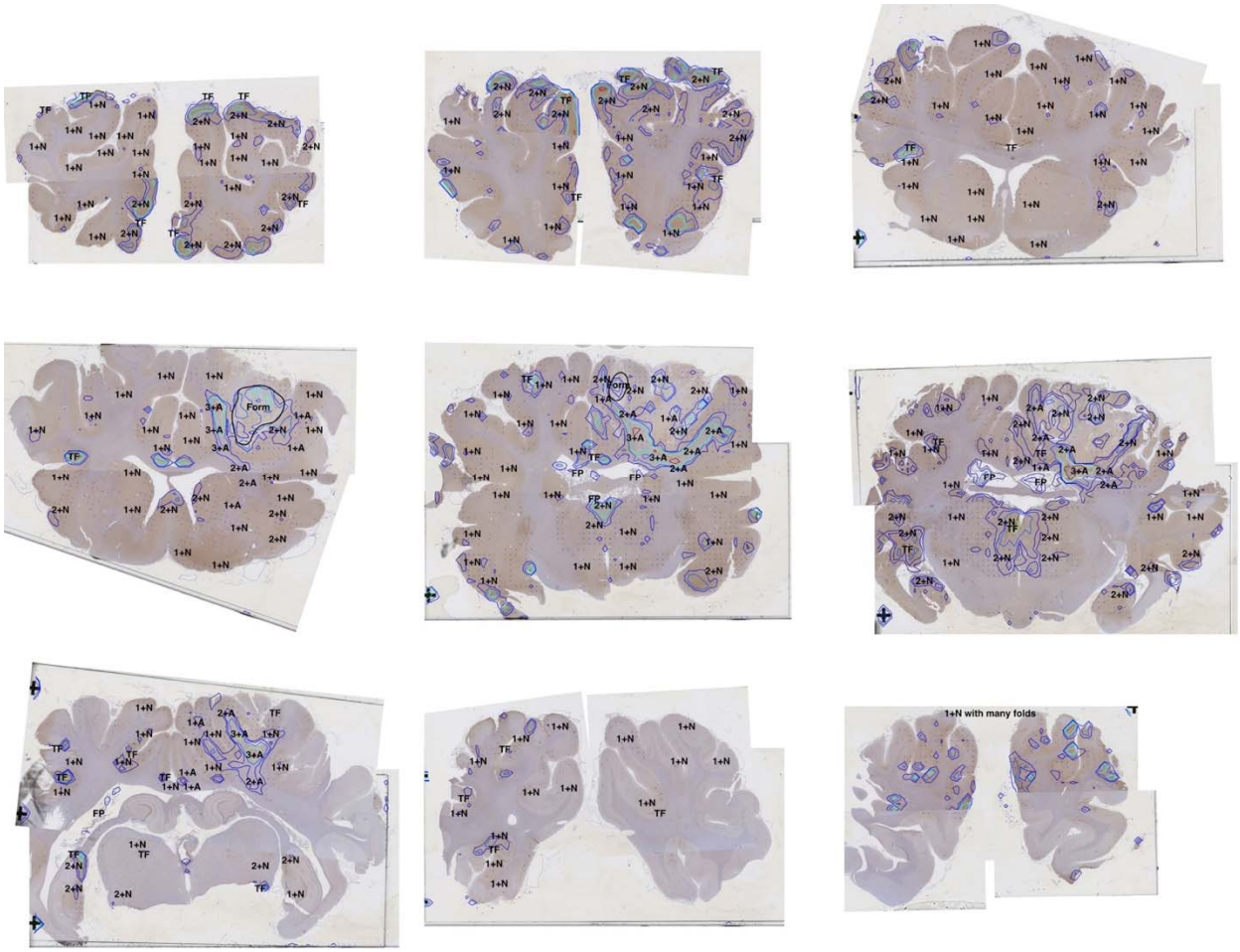

Fig 9. Injury levels on the coronal sections from Sheep B. Left to right, and top to bottom, levels 1 to 9. Each section is separated from each other by 5 mm. Contour levels are at 25, 50, 100, 200 and 500 counts per grid division. Dots show grid points with between 5 and 25 counts. Manual pathology markings are as follows: x+A indicates axonal injury at level x, x+N indicates neuronal injury at level x. Form represents an area of formalin pigmentation, H indicates a hole, FP indicates a false positive (due to extraneous DAB build up on the slide) and TF indicates an area of tissue folds.

Changed to –

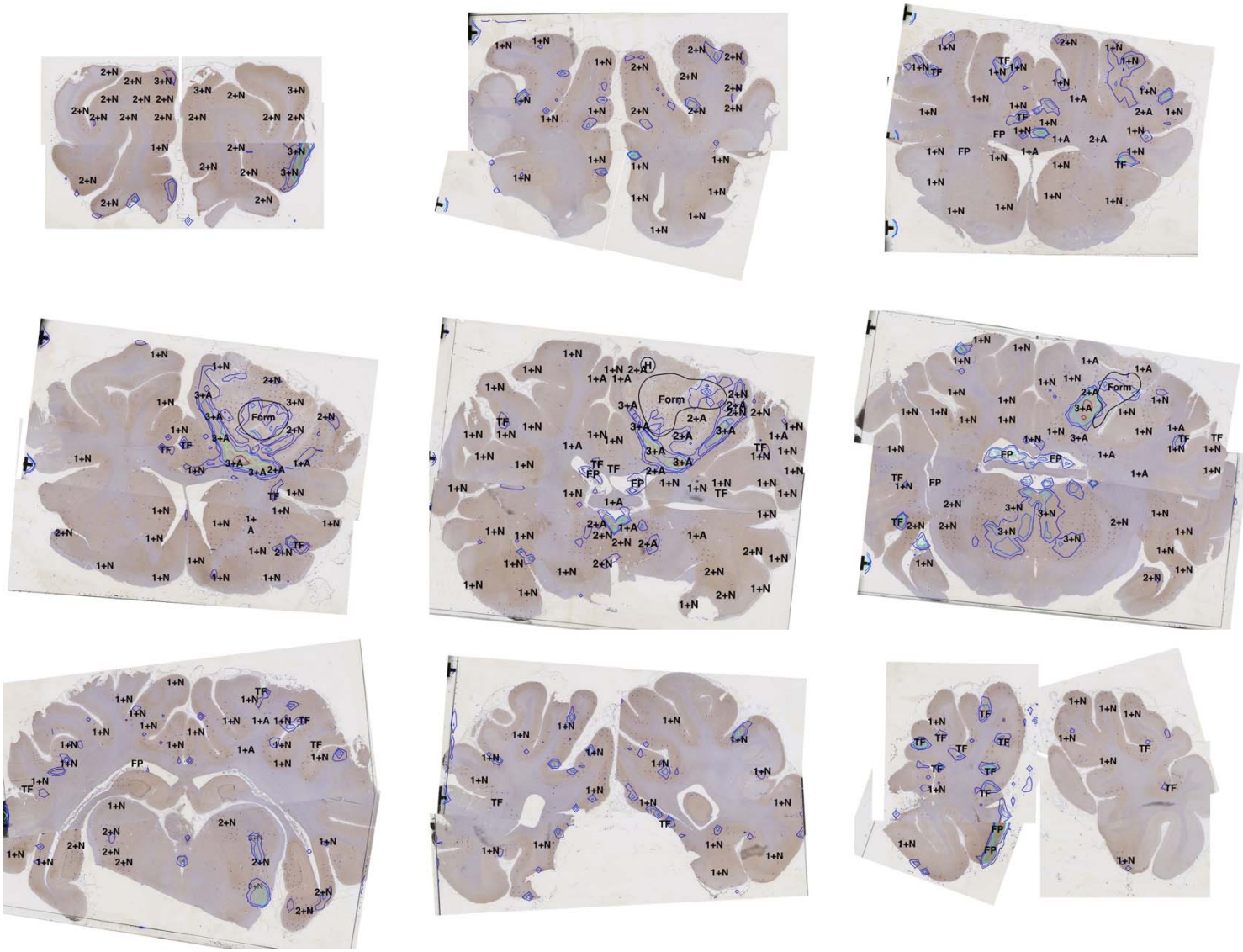

Fig 9. Injury levels on the coronal sections from Sheep B. Left to right, and top to bottom, levels 1 to 9. Each section is separated from each other by 5 mm. Contour levels are at 25, 50, 100, 200 and 500 counts per grid division. Dots show grid points with between 5 and 25 counts. Manual pathology markings are as follows: x+A indicates axonal injury at level x, x+N indicates neuronal injury at level x. Form represents an area of formalin pigmentation, H indicates a hole, FP indicates a false positive (due to extraneous DAB build up on the slide) and TF indicates an area of tissue folds.